Journal of Medical Imaging and Radiation Sciences 49 (2018) 286-292

Journal of Medical Imaging and Radiation Sciences

Journal de l'imagerie médicale et des sciences de la radiation

www.elsevier.com/locate/jmir

Research Article

2D Dose Reconstruction by Artificial Neural Network for Pretreatment Verification of IMRT Fields

Seied Rabie Mahdavi, PhD[a], Mohsen Bakhshandeh, PhD[b], Aram Rostami, PhD[a*] and Ali Jabbary Arfaee, MSc[c]

[a] *Department of Medical Physics, School of Medicine, Iran University of Medical Sciences, Tehran, Iran*
[b] *Department of Radiology Technology, School of Allied Medicine, Shahid Beheshti University of Medical Sciences, Tehran, Iran*
[c] *Shohada-e-Tajrish Hospital, Shahid Beheshti University of Medical Sciences, Tehran, Iran*

ABSTRACT

The use of intensity-modulated radiation therapy (IMRT) is developing rapidly in clinical routines. Because of the high complexity and uniqueness of IMRT treatment plans, patient-specific pretreatment quality assurance is generally considered a necessary prerequisite for patient treatment. In this work, we proposed a modified methodology of electronic portal imaging device (EPID)–based dose validation for pretreatment verification of IMRT fields by applying artificial neural networks (ANNs). The ANN must be trained and validated before use for pretreatment dose verification. For this purpose, 20 EPID fluence maps of IMRT prostate anterior-posterior fields were used as an input for ANN (feed forward type) and a dose map of those fluence maps that were predicted by treatment planning system as an output for ANN. After the training and validation of the neural network, the analysis of 10 IMRT prostate anterior-posterior fields showed excellent agreement between ANN output and dose map predicted by the treatment planning system. The average overall fields pass rate was 96.0% ± 0.1% with 3 mm/3% criteria. The results indicated that the ANN can be used as a low-cost, fast, and powerful tool for pretreatment dose verification, based on an EPID fluence map.

RÉSUMÉ

L'utilisation de la radiothérapie avec modulation d'intensité (RTMI) se développe rapidement dans la routine clinique. En raison de la grande complexité et du caractère unique des plans de traitement en RTMI, l'assurance de qualité préalable au traitement et spécifique au patient est généralement considérée comme un prérequis nécessaire au traitement. Dans cette étude, nous proposons une méthodologie modifiée de validation de dose basée sur appareil d'imagerie à portail électronique (EPID) pour la vérification avant traitement par l'application de réseaux neuronaux artificiels (RNN). Le RNN doit être entraîné et validé avant son utilisation pour la vérification de la dose avant le traitement. À cette fin, 20 cartes de fluence EPID de champ antéropostérieur (AP) de la prostate en RCMI ont été utilisés comme intrants pour le RNN (de type chargement en avant) et une carte de doses de ces cartes de fluence ayant été prédites par le système de planification de traitement (SPT) a été utilisée comme sortie pour le RNN. Après l'entraînement et la validation du réseau neural, l'analyse de dix champs AP de la prostate en RCMI a montré un excellent accord entre la sortie du RNN et la carte de doses prédite par le SPT. Le taux de réussite moyen global des champs était de 96,0% ± 0,1% avec un critère de 3 mm/3%. Les résultats indiquent que le RNN peut être utilisé comme outil rapide, puissant et peu coûteux pour la vérification de la dose avant le traitement, à partir d'une carte de fluence EPID.

Keywords: Artificial neural network; electronic portal imaging device; dose verification; intensity modulated radiation therapy

Introduction

The use of intensity-modulated radiation therapy (IMRT) is developing rapidly in clinical routine, and the advantages of this technique include better target coverage along with better sparing of organs at risk, improved target conformity, particularly for concave target volumes, and delivery of ablative radiation doses with a rapid fall-off [1]. Because of the high complexity and uniqueness of IMRT treatment plans, patient-specific pretreatment quality assurance is generally considered a prerequisite for patient treatment [2]. The most widely used form of pretreatment quality assurance for IMRT

* Corresponding author: Aram Rostami, PhD student of Medical Physics, Department of Medical Physics, School of Medicine, Iran University of Medical Sciences, Tehran, Iran.
E-mail address: Rostamy_1969@yahoo.com (A. Rostami).

1939-8654/$ - see front matter
https://doi.org/10.1016/j.jmir.2018.05.004

generally consists of absolute and 2D-dose measurements (with ionization chamber, diode, thermoluminescent dosimeter, radiographic and radiochromic film, etc.) [1,3,4]. Another approach to IMRT dose verification is the use of various matrix detectors that have been produced to measure energy fluence or absorbed dose in two dimensions [5,6]. Commercial options are available based on different measurement techniques. These include two-dimensional detectors, consisting of a large number of ionization chambers [7,8], or diodes [9,10] placed in a regularly spaced array or at specific points in a phantom [5]. A possible drawback of these devices is that they have relatively few measuring points and, so, a low spatial resolution. Another drawback of these devices is that they are time-consuming involving recalculation of the IMRT plan, temperature dependency, and set-up time on the linear accelerator [2,8].

The use of electronic portal imaging devices (EPIDs) is also of interest for IMRT verification [11]. Studies of the basic dosimetric performance of EPIDs have been presented for camera-based, liquid ionization, and amorphous silicon (a-Si) flat-panel systems [11–13]. Compared with other dosimetry devices, EPIDs—which are normally attached to linear accelerators—have no need for additional hardware to perform portal dosimetry. EPID measurements can be performed with minimum set-up requirements, and a 2D dose conversion can be performed immediately using digital raw data [14].

In general, two approaches have been adopted for the calibration of an EPID for dose measurements: conversion of the grayscale pixel value to a dose value and simulation (or prediction) of the grayscale pixel value [15]. These approaches must be validated in nonreference conditions—in particular, the robustness of these calibration models needs to be tested under various different clinical situations. Another drawback of these methods is its need for a detailed model of the EPID. However, accurate technical details are not always available, and, moreover, these methods require time and very complex calculation algorithms [15].

In this work, we proposed a modified methodology of EPID-based dose validation for pretreatment verification of IMRT fields through the application of artificial neural networks (ANNs). Fluence maps of IMRT prostate anterior-posterior (AP) treatment fields (without patient) obtained by EPID were used as inputs for ANN and a dose map of those fluence maps, predicted by treatment planning system (TPS) were used as an output for ANN in training phase.

ANN and machine-learning algorithms have been widely used for many pattern recognition problems in clinical and radiation therapy applications; the results have demonstrated that ANNs have good accuracy and high speed in response to complex problems and situations [16–27]. An ANN is a system composed of many simple interconnected processing elements (artificial neurons) operating in parallel, the function of which is determined by the network structure, the connection strengths, and the computation performed at the processing elements. An artificial neuron is a mathematical, nonlinear operator, which receives one or more inputs and computes a (usually weighted) sum of the inputs to produce a single output. Generally, this sum is passed through a nonlinear function, known as the activation function. An ANN approach has some inherent capabilities which other programming techniques lack. They are naturally parallel and so hold the promise of being able to solve intricate problems. The use of ANN requires a low memory storage, and very short time response once the network is trained [18,20].

Materials and Methods

Equipment

A linear accelerator with a 6 MV X-ray beam and dose rate of 400 monitor units per minute (Varian Unique) equipped with 80-leaf Varian millennium multileaf collimator was used. An a-Si–based a-Si1000 EPID (Portal vision; Varian Medical Systems, Palo Alto, USA) was used to acquire images. The Portal Vision a-Si1000 flat-panel EPID has a 40 × 30 cm^2 detecting surface with a matrix of 1024 × 768 pixels (0.392-mm pixel pitch). Each pixel consists of a light-sensitive photodiode and a thin film transistor to enable readouts. Overlying the array is a copper plate (of 1 mm thickness) and a scintillating layer (gadolinium oxysulphide) [13,28], making the portal imager an indirect detection system. The phosphor scintillator converts incident radiation into optical photons, enhancing the sensitivity of the detector more than 10-fold. The electric charge generated by the incident optical photons is accumulated in the photodiode until the signal is read out and digitized through an analog-to-digital converter [29]. The total water-equivalent thickness of the construction materials in front of the photodiodes is 8 mm, as specified by the manufacturer.

Eclipse (version 13.6) TPS (Varian Medical Systems, Palo Alto, USA) was used to calculate dose distributions of IMRT fields. The IMRT 2D dose map was calculated for 30 AP treatment fields of different prostate cases and after that, 2D dose maps converted in the 2-cm depth of cubic phantom with 25 cm and 30 cm length made of virtual water. The grid size, for both the fluence (image) and dose maps, was 0.5 cm, and an analytical anisotropic algorithm was used in the TPS.

2D Dose IMRT Fields Acquisition

In this study, 11,837 pixels of 20 dynamic IMRT prostate AP treatment fields (without patient) were used for training and validation of ANN. Dose per fraction, number of fraction, grid size for dose calculation, algorithm of plan optimization, and dose constrain for planning target volume and organs at risk were same for all of IMRT prostate plans. The pixels of 15 IMRT prostate AP fields were used for the training of the ANN. For validation phase and response evaluations of ANNs, we used pixels of 5 and 10 IMRT prostate AP fields respectively. All IMRT treatment fields were delivered to the linac treatment console via the ARIA record and verification system (Varian Medical Systems, Palo Alto, USA).

EPID Setup and Acquisition of Fluence Maps

The thickness of the construction material in front of the photodiodes is 1.5 cm (water-equivalent thickness is 8 mm). All IMRT EPID images (fluence map) were acquired at source EPID distance of 98.5 cm with 1.2 cm water equivalent additional buildup, in 2 cm water equivalent (behind the buildup region of 6 MV X-ray in water); the maximum frame acquisition rate was 9.574 frames/s (see Figure 1). When the EPID is used for dosimetry applications, such as pretreatment verification of the intensity-modulated beams, sufficient buildup needs to be applied to eliminate the contribution of scattered electrons to the dosimetric image [12]. An absence of buildup during the measurement will generate large deviations between acquired and expected images, inhibiting both the relative and absolute evaluations of the dynamic delivery. For this reason, we used sufficient buildup for image acquisition. This work can improve the precision of neural network responses.

Dark-field and flood-field calibration were performed for EPID before image acquisition. Dark-field calibration characterized the EPID response when there is no radiation beam. Flood-field calibration was also conducted to normalize the value of each individual pixel and achieve uniform spatial response of the EPID. Images of EPID were acquired in the integrated mode and were saved in dicom format.

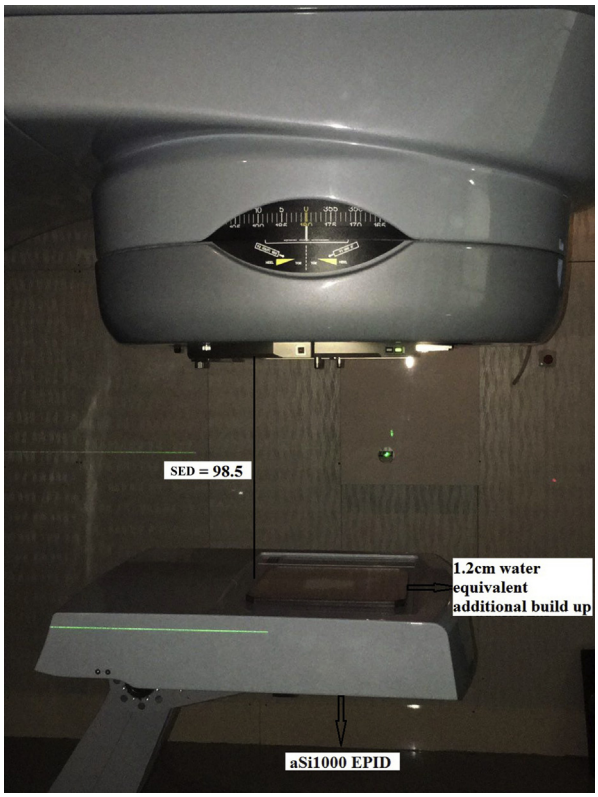

Figure 1. Setup of a-Si1000 electronic portal imaging device for acquisition fluence maps of intensity-modulated radiation therapy plan anterior-posterior fields with 1.2 cm water equivalent additional buildup in source electronic portal imaging device distance (SED) = 98.5 cm.

The Architecture of the Neural Network

To convert a 2D fluence map to a 2D dose map, in this study (total time needed to do this was about 5 minutes), we used feed forward (FF) multilayer ANN. The FF is a kind of backpropagation NN. This study used a Levenberg-Marquardt algorithm for FF-ANN training. The backpropagation NN is essentially a network of simple processing elements working together to produce a complex output. These elements or nodes are arranged into different layers: input, hidden, and output. The input layer propagated a particular input vector's components to hidden layers. Hidden layers, which are neuron nodes stacked in between inputs and outputs, allow neural networks to learn more complicated features and compute output values, which become inputs to the output layer. The output layer computes the network output for the particular input vector. In training phase, ANN produces an output vector for given input vector based on the current state of the network weights. The training set is repeatedly presented to network, and the weight values are adjusted in training set [17,23]. The structure of the neural network model we used in this study contains seven nodes for the input layer, three hidden layers, and an output layer that leads to the terminal response. The input layer has seven nodes (see Figure 2) that consisted of pixel coordinates (i, j), pixel intensity X(i, j), row distance of target pixel from central pixel F(i), and column distance of target pixel from central pixel F(j) and X(i–1, j), X(i+1, j), X(i, j–1), X(i, j+1), which are the neighboring pixel intensities of the target pixels. The accuracy of the network can be improved by introducing neighboring pixels [26,30].

There are three hidden layers in our model. It has been theoretically proven that a maximum of three hidden layers

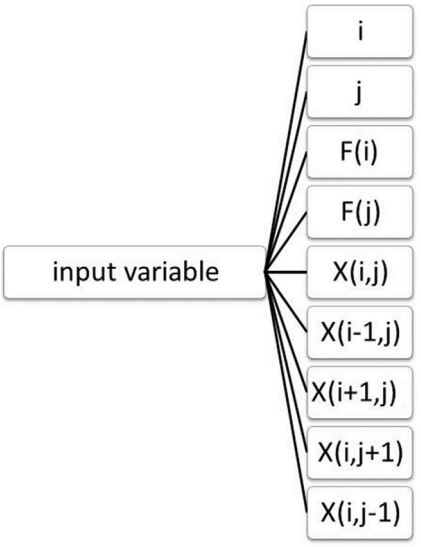

Figure 2. The schematic presentation of input variables of feed forward–artificial neural network contains pixel coordinates (i, j), pixel intensity X(i, j), row distance of target pixel from central pixel F(i), and column distance of target pixel from central pixel F(j) and X(i–1, j), X(i+1, j), X(i, j–1), X(i, j+1), which are the neighboring pixel intensities of target pixels.

is sufficient to arbitrarily approach any continuous function [25–30]. To find the numbers of sufficient hidden layers for our designed ANN, the best convergence between training and test data was considered. Initially, we started to solve the problem by using NN with only a single hidden layer. With one hidden layer, convergence did not occur after training. We then added one more hidden layer because the situation aforementioned shows that the continuous function, which was to be approached, is too complicated. Adding one hidden layer showed an increase in the convergence of the performance of the network. In this investigation, we found that three hidden layers have more sufficient performance than one and two hidden layers, and the regression of the network is more than 0.95% for random points (see Figure 3). The output layer of the ANN is the layer that gives a terminal response, which is a 2D dose modeled by an ANN.

We noticed that after 258 epochs, the performance of the ANN did not change significantly, and sufficient convergence between training and test data was obtained and best training performance (minimum mean square error) seen at epoch 6 (Figure 4). Design, training and testing of ANN, and data processing were performed with MATLAB software (version 8.5; MathWorks, USA).

Results

ANN 2D Dose Maps

Pixels of 5 and 10 IMRT prostate AP fields were used for validation and response evaluations of ANNs. Regression between the pixel intensity of 2D dose map predicted by the TPS (target) and pixel intensity of 2D dose map modeled by ANN (output) data is more than 0.95% so that this regression value indicated the ANN has received enough input values (11,837 pixels of 20 dynamic IMRT prostate AP treatment fields) in training and validation phase and ANN to be validated and ready for good responses (see Figure 5). After training and validation, ANN modeled the 2D dose map of the fluence map from EPID. A 2D dose map modeled by the ANN is shown by Figure 6.

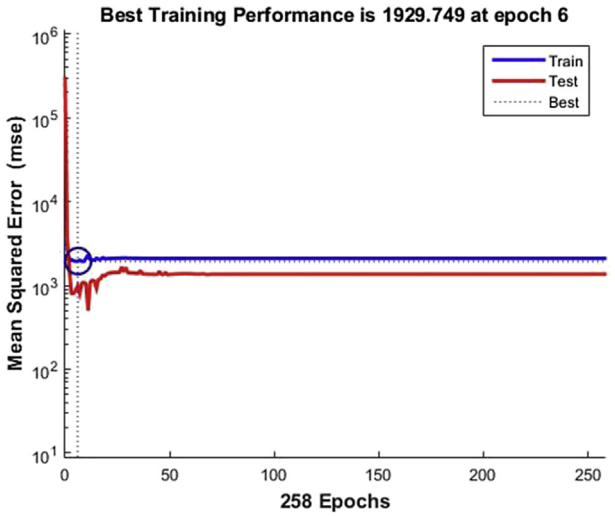

Figure 4. Performance of artificial neural network architectures for the same set of training shows sufficient convergence between training and test data, best training performance seen at epoch 6.

Gamma Evaluation of Neural Network Model

To compare the ANN 2D dose map with that from the TPS, we normalized the ANN dose map to its maximum dose. Similarly, the 2D dose map from the TPS was normalized to the maximum dose. The gamma evaluation of the TPS 2D dose prediction and the 2D dose modeled by ANN of 10 AP treatment fields of prostate IMRT indicate very similar results. The average overall fields pass rate was more than 95%, when the distance to agreement was (less than or equal to symbol) 3 mm and a dose difference (DD) of (less than or equal to symbol) 3% criteria were used.

Figure 7 shows the analysis of the 2D dose map with 0.5-cm grid size, as acquired with the TPS and the ANN. In Figures 7A, and B, 2D dose distributions of the TPS and ANN are respectively shown. Figure 7C shows a horizontal profile comparison between the TPS and ANN, and in Figure. 7D, a dose line profile comparison indicates 96.0% ± 0.1% pass rate for gamma evaluation of 3 mm/3%.

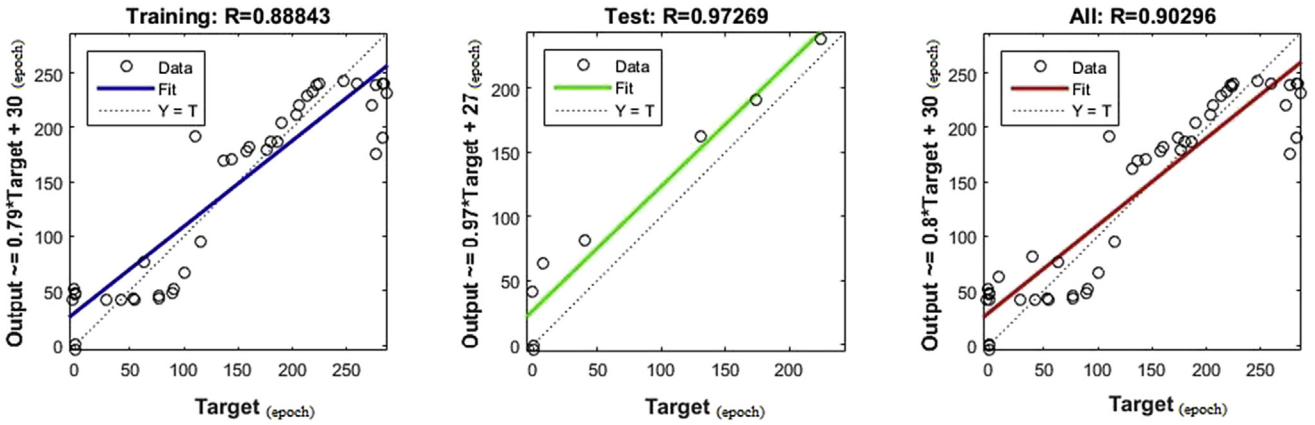

Figure 3. The regression value of network for training (R = 0.88843) and test phase (R = 0.97269) of artificial neural network (random point). The regression value for all (training and test) is 0.90296.

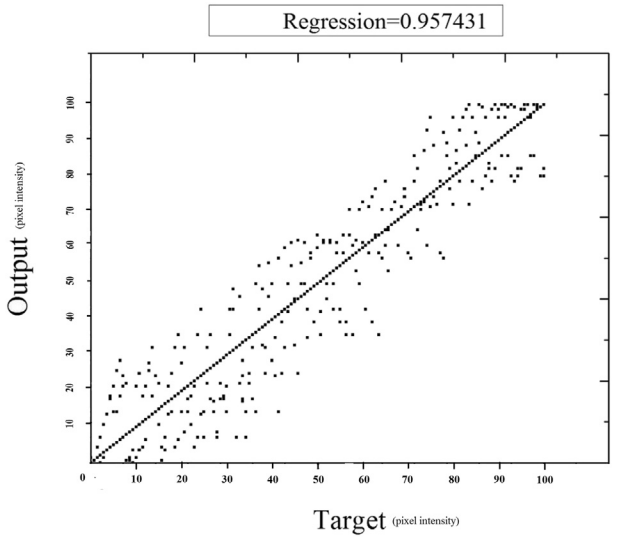

Figure 5. Regression line between target (2D dose map predicted by the treatment planning system) and output (2D dose map modeled by artificial neural network) data in validation phase of designed artificial neural network was 0.957431.

When the distance to agreement and DD were restricted to 2 mm/2% and 1 mm/1%, passing rates dropped to 94.3% ± 0.4% and 86.4% ± 1.4%, respectively. It means that the average pass rates decreases when the criteria are made tighter, as would be expected.

To evaluate the robustness and accuracy of the trained ANN, we took trained ANN (as described in 2.1 Section) under stress condition. In this phase of study, we recalculated 2D dose of 10 IMRT prostate AP fields predicted by the TPS with different grid sizes of, 0.4 cm, 0.3 cm, 0.2 cm, and 0.1 cm, and gamma evaluation was used for comparing 2D dose map of them with 2D dose map modeled by trained ANN. Results were summarized in Table 1; for all grid sizes, it can be seen that average gamma values pass rates do not have significant change when the 2D dose map grid sizes are lower.

Discussion

Other previous studies used ANN for modeling 2D dose distribution, percentage depth dose, and dose profiles of different fields [23–27]. In this study, we used a simple improved method for portal dosimetry with the help of ANN for the pretreatment verification of IMRT treatment.

The ability of ANN to model a 2D dose map, based on a fluence map obtained by a-Si1000 EPID, was evaluated in this study. Twenty fluence maps of IMRT prostate AP treatment fields (without patient) obtained by EPID were used as inputs for ANN (feed forward type) and a dose map of those fluence maps, predicted by the TPS as an output for ANN in the training and validation phase. After the training and validation of neural networks, the analysis of 10 IMRT prostate AP fields plans that were not seen earlier by trained ANNs, showed excellent agreement between the ANN 2D dose map modeled and the dose map predicted by the TPS. The average overall fields pass rate was more than 95% when 3 mm/3% criteria were used. This index value for 3 mm/3% criteria is comparable with a very complex portal dosimetry method and expensive commercial portal dosimetry software [15].

In similar study, Kalantzis et al [30] imported fluence maps, which were acquired by a-Si1000 (Varian Medical Systems, Palo Alto, USA) to the Pinnacle TPS (Philips Radiation Oncology Systems, Fitchburg, WI) to calculate the 2D dose maps of the horizontal isocenter plane of a homogeneous virtual cylindrical phantom. In this study, 2D dose predicted by the TPS depends on the fluence map acquired by EPID. All the fluence map measurements in study of Kalantzis et al were performed without additional buildup that can be impressed by scattered electrons and high gradient dose region. As these conditions are a source of uncertainty in dose measurement and in the TPS prediction, they should ideally be avoided [12]. All IMRT EPID images in our study (fluence maps) were acquired with sufficient buildup materials (totally: 2 water equivalent buildup) and the 2D dose map predicted by the TPS is independent of the fluence map. On other

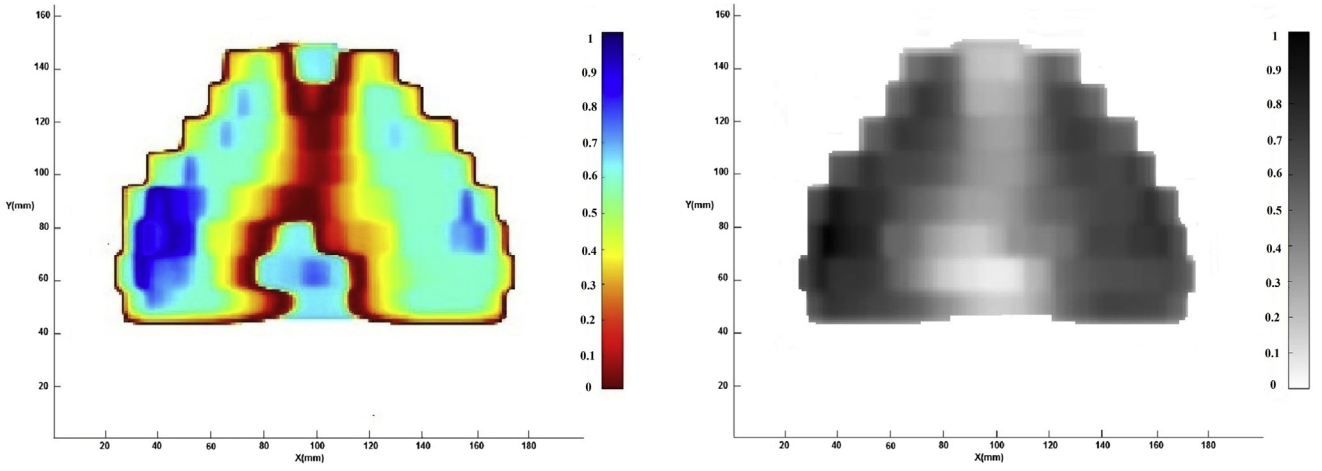

Figure 6. The artificial neural network (ANN) modeled the 2D dose map of the fluence map from electronic portal imaging device. The fluence map electronic portal imaging device that was used as input for ANN (right), 2D dose map modeled by ANN (left).

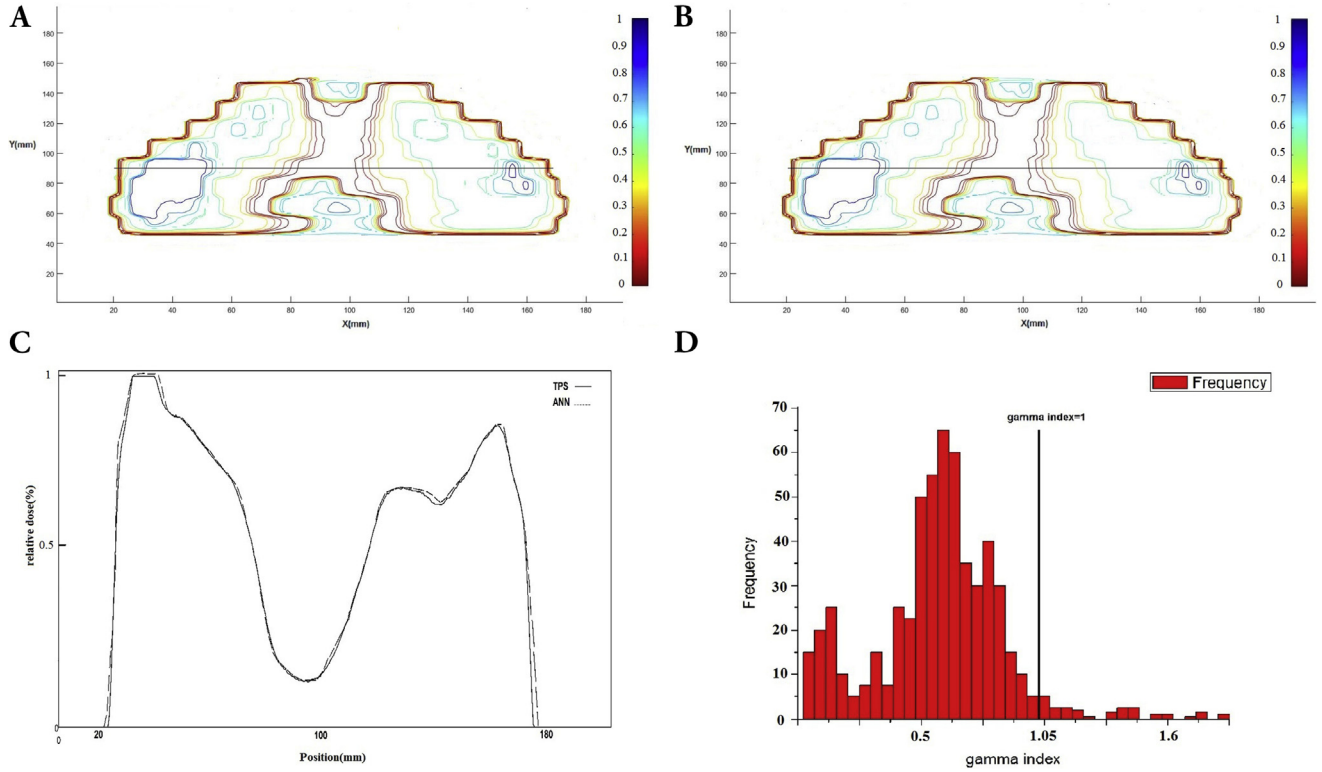

Figure 7. A, Isodose profile for 2D dose of the treatment planning system; B, isodose profile for 2D dose reconstructed by artificial neural network; C, horizontal dose line profile comparison between the TPS and artificial neural network; D, 2D gamma index histogram; and 96% of gamma index value are smaller than 1.

advantage of the designed ANN in our study, in comparison with similar studies [26–30], is that a uniquely trained ANN can model a 2D dose map, and it does not require any design for two neural networks of low- and high-dose gradient regions on a 2D dose map. The results of this study indicated that one NN can model the total region of a 2D dose map (low-dose and high-dose regions) if trained with appropriate node(s) for input layer, hidden layer, and optimize iteration. The suitable and optimized responses of our designed neural network can be because of the precise introduction of pixels coordination and distances from central pixel and also the introduction of four neighbors' pixel intensities.

Good response and performance of ANN trained by 2D dose map with 0.5 cm grid size in comparison of 2D dose predicted by the TPS with different grid sizes indicated robustness and accuracy of ANN in different and more stringent conditions. This phase of the study increases our confidence about the performance of trained ANN in different stress conditions that have been previously been encountered by the ANN.

The extension of our method would be to evaluate the ability of ANNs to predict the dose intensity for in vivo dosimetry in heterogeneous irradiation fields for different clinical situations.

Another extension of our method can use different modulated IMRT fields and the evaluated ability of NN performance in different modulated IMRT fields, ranging from relatively less modulated IMRT fields of prostate cases to highly modulated fields for head and neck cases. Another way to extend and evaluate ANN ability for portal dosimetry is to use different NN and compare their abilities for this task.

Table 1
Gamma Index Evaluation Between 2D Dose Map Modeled by Trained ANN and 2D Dose Map Predicted by the TPS with 0.5 cm, 0.4 cm, 0.3 cm, 0.2 cm, and 0.1 cm Grid Size: Pass Rate with Gamma Evaluation of 3 mm/3%, 2 mm/2% and 1 mm/1%

Gamma Criteria			2D Dose Map Grid Size (cm)
1 mm/1%	2 mm/2%	3 mm/3%	
86.4% ± 1.4%	94.3% ± 0.4%	96.0% ± 0.1%	0.5
86.1% ± 1.1%	94.1% ± 0.3%	95.9% ± 0.2%	0.4
85.9% ± 1.3%	93.9% ± 0.5%	95.7% ± 0.1%	0.3
85.8% ± 1.4%	93.7% ± 0.5%	95.5% ± 0.2%	0.2
85.4% ± 0.9%	93.0% ± 0.4%	95.3% ± 0.2%	0.1

Conclusion

The results of this study showed the ability of the ANN as a powerful tool for 2D dose reconstruction-based image acquisition of EPID for IMRT fields without patients. In addition, the results indicate that the low-cost method used in this study is a precise and high-speed method for the pretreatment verification of IMRT treatment.

In future studies, we will want to use a 2D dose map measured by qualifying a 2D array dosimeter as an output of NN and comparing a 2D dose map modeled by this method with a 2D dose map predicted by the TPS for the same IMRT fields.

Footnotes

Contributors: All authors contributed to the conception or design of the work, the acquisition, analysis, or interpretation of the data. All authors were involved in drafting and commenting on the paper and have approved the final version.

Funding: This study did not receive any specific grant from funding agencies in the public, commercial, or not-for-profit sectors.

Competing interests: All authors have completed the ICMJE uniform disclosure form at www.icmje.org/coi_disclosure.pdf and declare: no financial relationships with any organizations that might have an interest in the submitted work in the previous three years; no other relationships or activities that could appear to have influenced the submitted work.

Ethical approval: Requirement of Research Ethics Board approval for this project was not required, as there was no patient involvement.

References

[1] Van Esch, A., Bohsung, J., Sorvari, P., Tenhunen, M., Paiusco, M., & Iori, M. (2002). Acceptance tests and quality control procedures for the clinical implementation of intensity modulated radiotherapy (IMRT) using inverse planning and sliding windows technique: experience from five radiotherapy departments. *Radiother Oncol* 65, 53–70.

[2] Burman, C., Chui, C., & Kutcher, G., et al. (1997). Planning delivery and quality assurance of intensity-modulated radiotherapy using dynamic multileaf collimator: a strategy for large-scale implementation for the treatment of carcinoma of the prostate. *Int J Radiat Oncol Biol Phys* 39, 863–873.

[3] Van Elmpt, W. J., Nijsten, S. M., Mijnheer, B. J., Dekker, A. L., & Lambin, P. (2007). The next step in patientspecific QA: 3D dose verification for conformal and intensity modulated RT based on EPID dosimetry and monte carlo calculations. *Int J Radiat Oncol Biol Phys* 69, 672–673.

[4] Sadagopan, R., Bencomo, J. A., Martin, R. L., Nilsson, G., Matzen, T., & Balter, P. A. (2009). Characterization and clinical evaluation of a novel IMRT quality assurance system. *J Appl Clin Med Phys* 10, 104–119.

[5] Poppe, B., Blechschmidt, A., & Djouguela, A., et al. (2006). Two-dimensional ionization chamber arrays for IMRT plan verification. *Med Phys* 33, 1005–1015.

[6] Wiezorek, T., Banz, N., & Schwedas, M., et al. (2005). Dosimetric quality assurance for intensity-modulated radiotherapy feasibility study for a filmless approach. *Strahlenther Onkol* 181, 468–474.

[7] Amerio, S., Boriano, A., & Bourhaleb, F., et al. (2004). Dosimetric characterization of a large area pixel-segmented ionization chamber. *Med Phys* 31, 414–420.

[8] Spezi, E., Angelini, A. L., Romani, F., & Ferri, A. (2005). Characterization of a 2D ion chamber array for the verification of radiotherapy treatments. *Phys Med Biol* 50, 3361–3373.

[9] Letourneau, D., Gulam, M., Yan, D., Oldham, M., & Wong, J. W. (2004). Evaluation of a 2D diode array for IMRT quality assurance. *Radiother Oncol* 70, 199–206.

[10] Jursinic, P. A., & Nelms, B. E. (2003). A 2-D diode array and analysis software for verification of intensity modulated radiation therapy delivery. *Med Phys* 30, 870–879.

[11] Louwe, R. J., Tielenburg, R., Van Ingen, K. M., Mijnheer, B. J., & Van Herk, M. B. (2004). The stability of liquid-filled matrix ionization chamber electronic portal imaging devices for dosimetry purposes. *Med Phys* 31, 819–827.

[12] De Boer, J. C., Heijmen, B. J., Pasma, K. L., & Visser, A. G. (2000). Characterisation of a high-elbow, fluoroscopic electronic portal imaging device for portal dosimetry. *Phys Med Biol* 45, 197–216.

[13] Chang, C. S., Tseng, Y., Hwang, J. M., Shih, R., & Chuang, K. S. (2016). Dosimetric characteristics and day-to-day performance of an amorphous-silicon type electronic portal imaging device. *Radiat Meas* 91, 9–14.

[14] Lee, C., Menk, F., Cadman, P., & Greer, P. B. (2009). A simple approach to using an amorphous silicon EPID to verify IMRT planar dose maps. *Med Phys* 36, 984–992.

[15] Van Elmpt, W., Mcdermott, L., & Nijsten, S., et al. (2008). A literature review of electronic portal imaging for radiotherapy dosimetry. *Radiother Oncol* 88(3), 289–309.

[16] Zhu, X., Ge, Y., Li, T., Thongphiew, D., Yin, F., & Wu, Q. (2011). A planning evaluation tool for prostate adaptive IMRT based on machine learning. *Med Phys* 38, 719–726.

[17] Derong, L., Zhongyu, P., & Lloyd, S. R. (2007). A neural network method for detection of obstructive sleep apnea and narcolepsy on pupil size and EEG, IEEE. *Trans Neural Netw* 19, 308–318.

[18] Cenci, M., Nagar, C., & Vecchione, A. (2000). PAPNET-assisted primary screening of conventional cervical smears. *Anticancer Res* 20, 3887–3899.

[19] Reddy, M. S., Edenbrandt, L., Svensson, J., Haisty, W. K., & Pahlm, O. (1992). Neural network versus electrocardiographer and conventional computer criteria in diagnosing anterior infarct from the EEG. *Comput Cardiol* 11, 667–670.

[20] Yamashita, K., Yoshiura, T., & Arimura, H., et al. (2008). Performance evaluation of radiologists with artificial nerual netwok for differential diagnosis of intra-axial cerebral tumors on MR images. *Am J Neuroradiol* 29, 1153–1158.

[21] Chen, S., Zhou, S., Zhang, J., Yin, F., Marks, L., & Das, S. K. (2007). A neural network model to predict lung radiation-induced pneumonitis. *Med Phys* 34, 3420–3427.

[22] Gunturkun, R. (2010). Determining the amount of anesthetic medicine to be applied by using Elman's recurrent neural networks via resilient back propagation. *J Med Syst* 34, 493–497.

[23] Wu, X., & Zhu, Y. (2000). A neural network regression model for relative dose computation. *Phys Med Biol* 45, 913–922.

[24] Blake, S. (2004). Artificial neural network modeling of megavoltage photon dose distributions. *Phys Med Biol* 49, 2515–2526.

[25] Mathieu, R., Maritn, E., Gschwind, R., Makovicka, L., ContassotVinier, S., & Bahi, J. (2005). Calculations of dose distributions using a neural network model. *Phys Med Biol* 50, 1019–1028.

[26] Vasseur, A., Makovicka, L., Maritn, E., Sauget, M., Contassot-Vinier, S., & Bahi, J. (2008). Dose calculations using artificial neural networks: a feasibility study for photon beams. *Nucl Instrum Methods Phys Res B* 266, 1085–1093.

[27] Milan, J., & Bentley, R. E. (1974). The storage and masnipulation of radiation dose data in a small digital computer,. *Br J Radiol* 47, 115–121.

[28] Munro, P., & Bouius, D. C. (1998). X-ray quantum limited portal imaging using amorphous silicon flat-panel arrays. *Med Phys* 25, 689–702.

[29] El-Mohri, Y., Antonuk, L. E., & Yorkston, J., et al. (1999). Relative dosimetry using active matrix flat-panel imager (AMFPI) technology. *Med Phys* 26, 1530–1541.

[30] Kalantzis, G., Vasquez-Quino, L., Zalman, T., Pretx, G., & Lie, Y. (2011). Toward IMRT 2D dose modeling using artificial neural networks: a feasibility study. *Med Phys* 38, 5807–5817.